THERMAL AND DYNAMICAL FEATURES OF A THUNDERSTORM WITH A TILTED AXIS OF ROTATION

T. Theodore Fujita

Number 118
December 1973

MESOMETEOROLOGY PROJECT --- RESEARCH PAPERS

1.* Report on the Chicago Tornado of March 4, 1961 - Rodger A. Brown and Tetsuya Fujita

2.* Index to the NSSP Surface Network - Tetsuya Fujita

3.* Outline of a Technique for Precise Rectification of Satellite Cloud Photographs - Tetsuya Fujita

4.* Horizontal Structure of Mountain Winds - Henry A. Brown

5.* An Investigation of Developmental Processes of the Wake Depression Through Excess Pressure Analysis of Nocturnal Showers - Joseph L. Goldman

6.* Precipitation in the 1960 Flagstaff Mesometeorological Network - Kenneth A. Styber

7.** On a Method of Single- and Dual-Image Photogrammetry of Panoramic Aerial Photographs - Tetsuya Fujita

8. A Review of Researches on Analytical Mesometeorology - Tetsuya Fujita

9.* Meteorological Interpretations of Convective Nephsystems Appearing in TIROS Cloud Photographs - Tetsuya Fujita, Toshimitsu Ushijima, William A. Hass, and George T. Dellert, Jr.

10.* Study of the Development of Prefrontal Squall-Systems Using NSSP Network Data - Joseph L. Goldman

11. Analysis of Selected Aircraft Data from NSSP Operation, 1962 - Tetsuya Fujita

12. Study of a Long Condensation Trail Photographed by TIROS I - Toshimitsu Ushijima

13. A Technique for Precise Analysis of Satellite Data; Volume I - Photogrammetry (Published as MSL Report No. 14) - Tetsuya Fujita

14. Investigation of a Summer Jet Stream Using TIROS and Aerological Data - Kozo Ninomiya

15. Outline of a Theory and Examples for Precise Analysis of Satellite Radiation Data - Tetsuya Fujita

16. Preliminary Result of Analysis of the Cumulonimbus Cloud of April 21, 1961 - Tetsuya Fujita and James Arnold

17. A Technique for Precise Analysis of Satellite Photographs - Tetsuya Fujita

18.* Evaluation of Limb Darkening from TIROS III Radiation Data - S.H.H. Larsen, Tetsuya Fujita, and W.L. Fletcher

19. Synoptic Interpretation of TIROS III Measurements of Infrared Radiation - Finn Pedersen and Tetsuya Fujita

20.* TIROS III Measurements of Terrestrial Radiation and Reflected and Scattered Solar Radiation - S.H.H. Larsen, Tetsuya Fujita, and W.L. Fletcher

21. On the Low-level Structure of a Squall Line - Henry A. Brown

22.* Thunderstorms and the Low-level Jet - William D. Bonner

23.* The Mesoanalysis of an Organized Convective System - Henry A. Brown

24. Preliminary Radar and Photogrammetric Study of the Illinois Tornadoes of April 17 and 22, 1963 - Joseph L. Goldman and Tetsuya Fujita

25. Use of TIROS Pictures for Studies of the Internal Structure of Tropical Storms - Tetsuya Fujita with Rectified Pictures from TIROS I Orbit 125, R/O 128 - Toshimitsu Ushijima

26. An Experiment in the Determination of Geostrophic and Isallobaric Winds from NSSP Pressure Data - William Bonner

27. Proposed Mechanism of Hook Echo Formation - Tetsuya Fujita with a Preliminary Mesosynoptic Analysis of Tornado Cyclone Case of May 26, 1963 - Tetsuya Fujita and Robbi Stuhmer

28. The Decaying Stage of Hurricane Anna of July 1961 as Portrayed by TIROS Cloud Photographs and Infrared Radiation from the Top of the Storm - Tetsuya Fujita and James Arnold

29. A Technique for Precise Analysis of Satellite Data, Volume II - Radiation Analysis, Section 6. Fixed-Position Scanning - Tetsuya Fujita

30. Evaluation of Errors in the Graphical Rectification of Satellite Photographs - Tetsuya Fujita

31. Tables of Scan Nadir and Horizontal Angles - William D. Bonner

32. A Simplified Grid Technique for Determining Scan Lines Generated by the TIROS Scanning Radiometer - James E. Arnold

33. A Study of Cumulus Clouds over the Flagstaff Research Network with the Use of U-2 Photographs - Dorothy L. Bradbury and Tetsuya Fujita

34. The Scanning Printer and Its Application to Detailed Analysis of Satellite Radiation Data - Tetsuya Fujita

35. Synoptic Study of Cold Air Outbreak over the Mediterranean using Satellite Photographs and Radiation Data - Aasmund Rabbe and Tetsuya Fujita

36. Accurate Calibration of Doppler Winds for their use in the Computation of Mesoscale Wind Fields - Tetsuya Fujita

37. Proposed Operation of Intrumented Aircraft for Research on Moisture Fronts and Wake Depressions - Tetsuya Fujita and Dorothy L. Bradbury

38. Statistical and Kinematical Properties of the Low-level Jet Stream - William D. Bonner

39. The Illinois Tornadoes of 17 and 22 April 1963 - Joseph L. Goldman

40. Resolution of the Nimbus High Resolution Infrared Radiometer - Tetsuya Fujita and William R. Bandeen

41. On the Determination of the Exchange Coefficients in Convective Clouds - Rodger A. Brown

* Out of Print
** To be published

(Continued on back cover)

THERMAL AND DYNAMICAL FEATURES OF A THUNDERSTORM WITH A TILTED AXIS OF ROTATION

by

T. Theodore Fujita
The University of Chicago

SMRP Research Paper No. 118

December 1973

The research reported in this paper has been sponsored by the National Aeronautics and Space Administration under grant NGR 14-001-008.

THERMAL AND DYNAMICAL FEATURES OF A THUNDERSTORM WITH A TILTED AXIS OF ROTATION

T. Theodore Fujita
The University of Chicago

1. INTRODUCTION

The first sequence of radar pictures of a rotating thunderstorm in the shape of a rotating hook were obtained by the Illinois State Water Survey. [Refer to reports by Huff et al. (1954) and Fujita (1958).] Since then a large number of cloud photographs of the parent or mother clouds of tornadoes were obtained. One of the best examples of early storms is the Fargo tornado cloud of June 20, 1957. [Refer to Fujita (1960).] Recent developments in Doppler radar now permit one to scan the entire volume of a thunderstorm in an attempt to establish velocity vectors of hydrometeors. [Refer to Brown et al. (1973).]

It is a well-established concept that a thunderstorm, or a portion thereof rotates when an intense tornado forms. In other words, strong tornadoes tend to spawn from rotating thunderstorms. Despite an early presumption that the rotational axis is more or less vertical, observational evidence indicates a significant tilt. One of the best examples is the April 21, 1961 cloud photographed by Fujita from the Weather Bureau's DC-6 in a research flight mission. Although a sequence of pictures showing an apparent tilt was available, no research on the tilt was attempted until Dr. Robert Costen (1972) of NASA's Langley Research Center pointed out the importance of such

---

The research reported in this paper has been sponsored by the National Aeronautics and Space Administration under grant NGR 14-001-008.

a study. Thus, the data collected some 12 years ago were re-analyzed in an attempt to reconstruct the cloud features based on new ideas and assumptions.

2. TILT OF STORM AXIS

The three-dimensional tilt vector of a rotating thunderstorm can be determined by taking cloud pictures from different directions. An aircraft platform provides us with quickly changing views which can be used in the tilt computations.

The true tilt is defined as the direction of the cloud axis measured from the local vertical through the cloud. The tilt measured on a horizontal image may be called the apparent tilt, which is different from the true tilt. They can be related by an equation

$$\tan \tau_a = \tan \tau \sin (\alpha - \beta) \qquad (1)$$

where τ_a is the apparent tilt, τ is the true tilt, α is the azimuth of the cloud axis, and β is the azimuth of the cloud viewed from the aircraft.

The apparent tilt of the rotating thunderstorm of April 21, 1961, measured from six directions, is plotted in Fig. 1 as a function of the cloud azimuth β . As

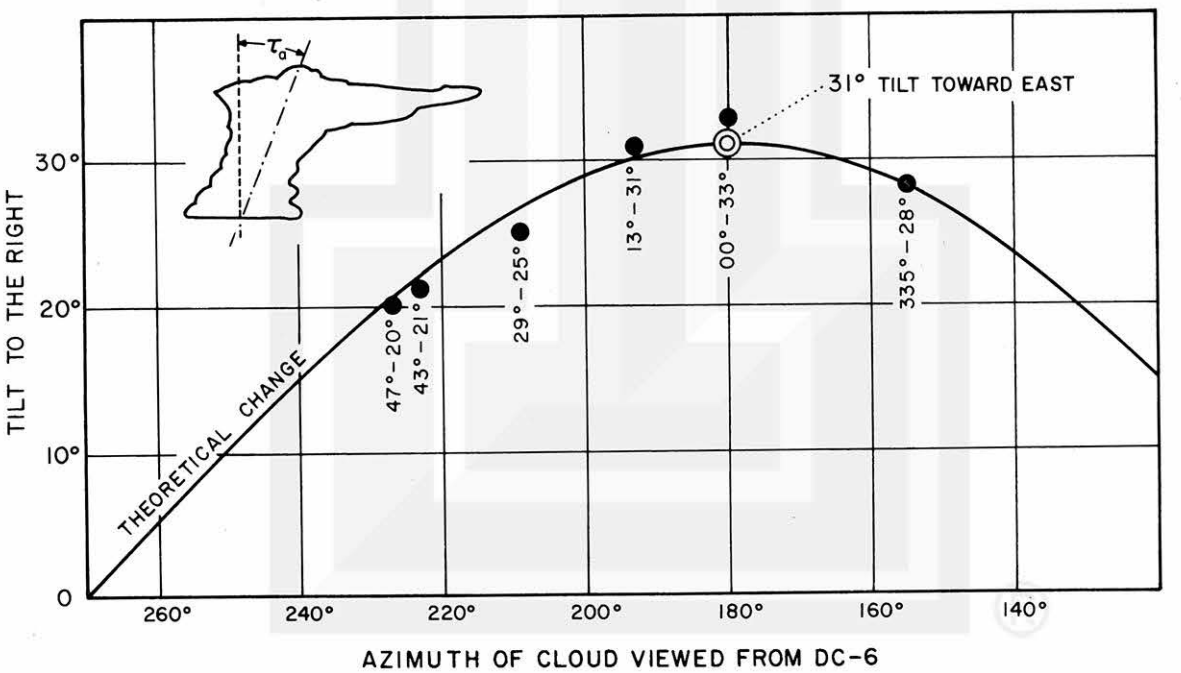

Fig. 1. Variation in the apparent tilt of a rotating thunderstorm.

shown in Eq. (1), the apparent tilt coincides with the true tilt when $\alpha - \beta = 90°$. In this case, the azimuth of the cloud was 0° when the apparent tilt reached the maximum value. This means that the cloud was tilted due eastward.

The variation of the apparent tilt due to the change in the viewing direction is shown in Figs. 2 and 3. Fig. 2 represents a view of the cloud toward the 43° azimuth;

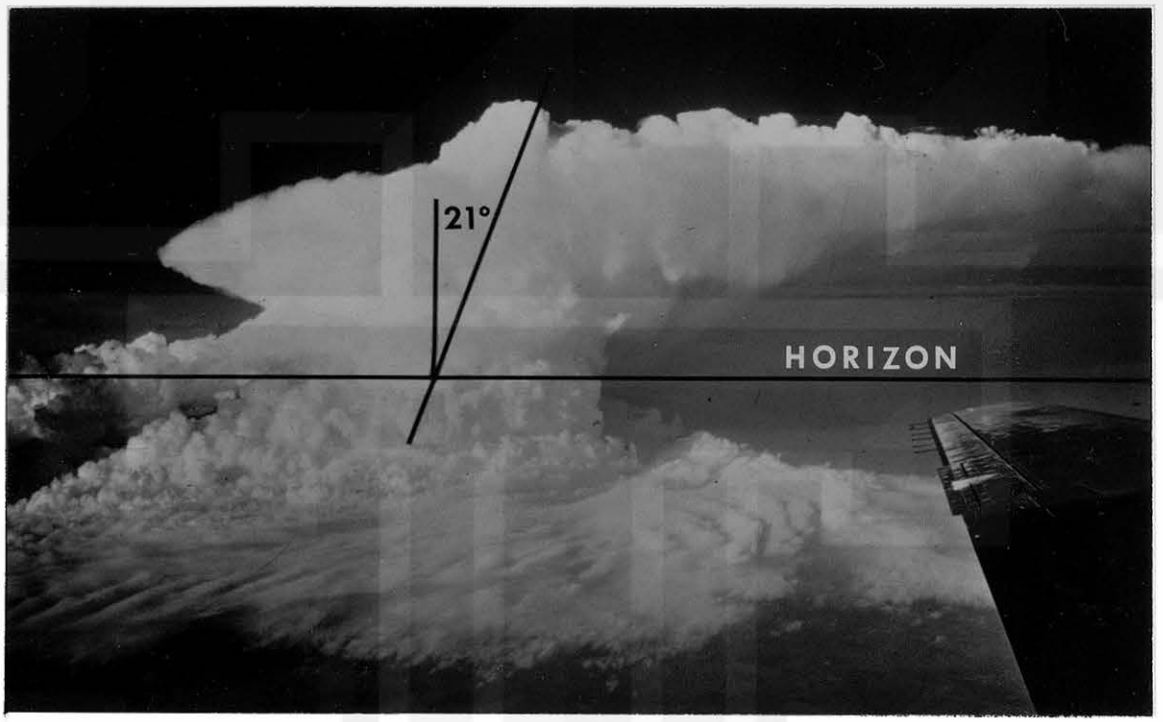

Fig. 2. A view toward the 43° azimuth.

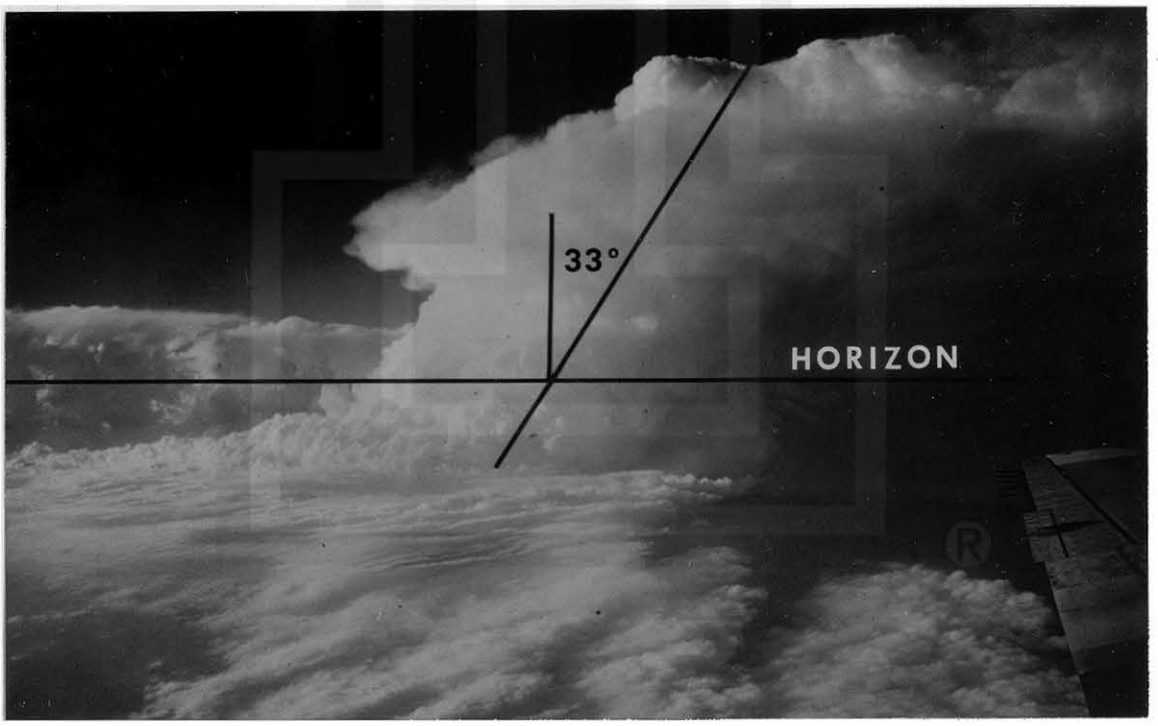

Fig. 3. A view toward the 00° azimuth or due north.

the apparent tilt is 21°. The cloud shows a cyclonic rotation at least near the cloud base. Fig. 3 is a view of the cloud with a 00°azimuth when the apparent tilt reached the maximum value of 33°. These figures clearly show the variation in the cloud tilt. The true tilt of 31° was obtained after smoothing the six values in Fig. 1.

3. ENVIRONMENTAL WINDS

The environmental flow must be known accurately in order to interpret the reasons for a tilt of 31°. This value appears to be rather large for such a large rotating thunderstorm. Unfortunately, no radiosonde station was located close enough to permit us to estimate the environmental wind from data of a single station. In order to estimate the best possible upper winds in the immediate vicinity of the cloud, a 6-layer analysis was performed as shown in Fig. 4.

The 850-mb wind at the cloud location was estimated to be 220°-32 kt. The flow at this level appears to be rather straight. As the height increases to 700 mb, the environmental flow started showing a definite anticyclonic curvature. The wind speed increased toward the north, resulting in a definite anticyclonic vorticity around the cloud. The 700 mb flow was 240°-40 kt.

At 500 mb, the flow became straight again with the velocity 250°-50 kt. At this level the streamlines diverged with a decreasing wind speed toward the east. A 275°-75 kt wind is seen at 300 mb where a definite anticyclonic flow is apparent. A jetstream flow was located near the 200 mb level with the 280°-105 kt wind. The jet axis was, however, seen far to the south, over central Oklahoma. The 100 mb level is located above the level of the maximum wind. At this level the wind speed decreased to only 55 kt from the west.

The environmental flow determined through the mandatory-level analyses is put together in the hodograph of Fig. 5. The surface, 900-mb, and 400-mb winds were estimated from other sources. The effective inflow wind is approximately 190°-40 kt located within a 3000-ft layer above the surface. The mean wind averaged between the cloud base at 4000 ft MSL and the 300 mb level was 240°-45 kt, and the cloud motion estimated to be 270°-22 kt was 30° to the right of the mean wind. This cloud was certainly a right-deviating storm. For further definition refer to Browning (1965) and Fujita (1965).

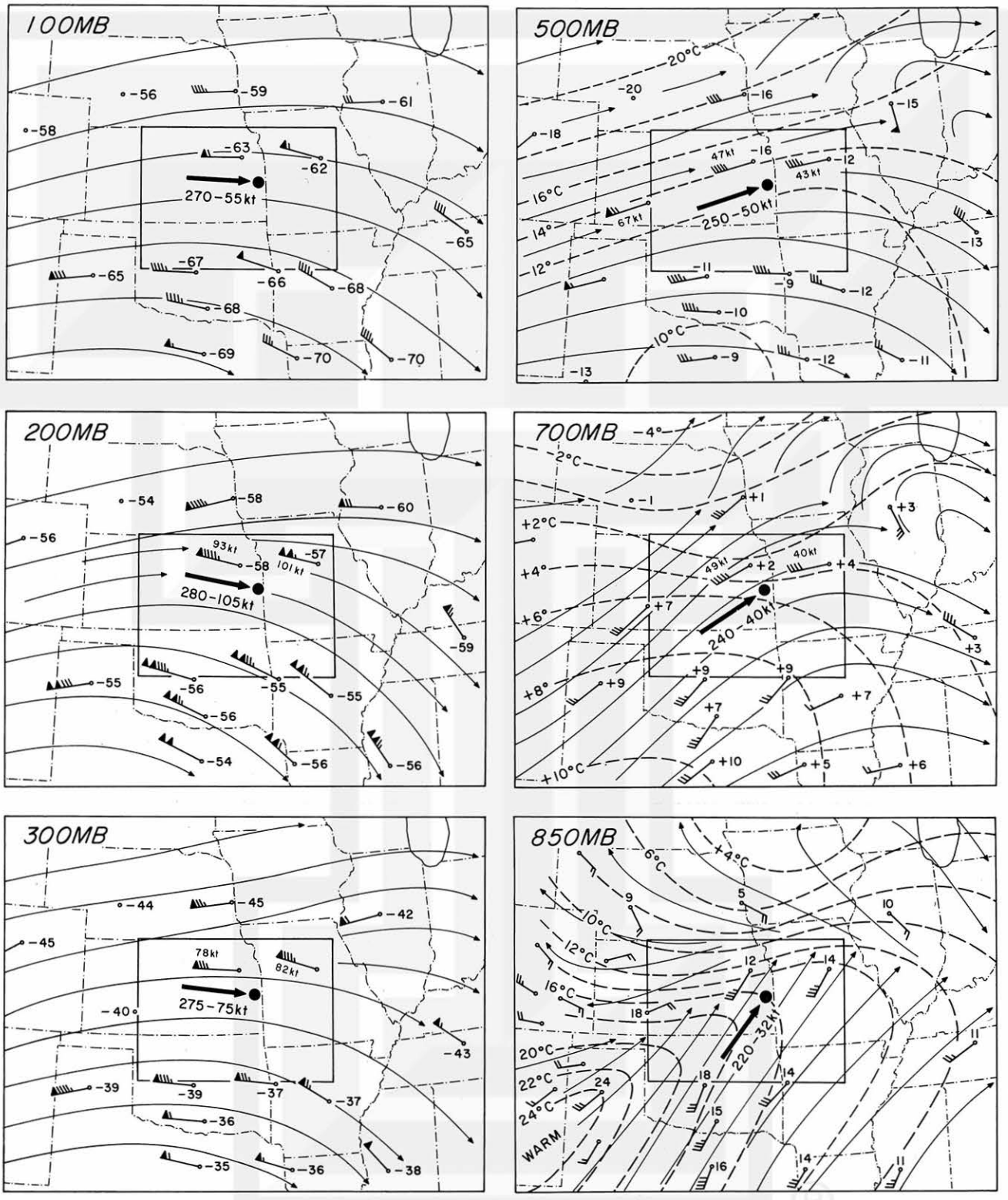

Fig. 4. Multi-level analysis of wind and temperature fields around the rotating thunderstorm of April 21, 1961. The map time is 1800 CST, when the storm was in the mature stage. Hourly surface maps within the boxed area appear in Fig. 8.

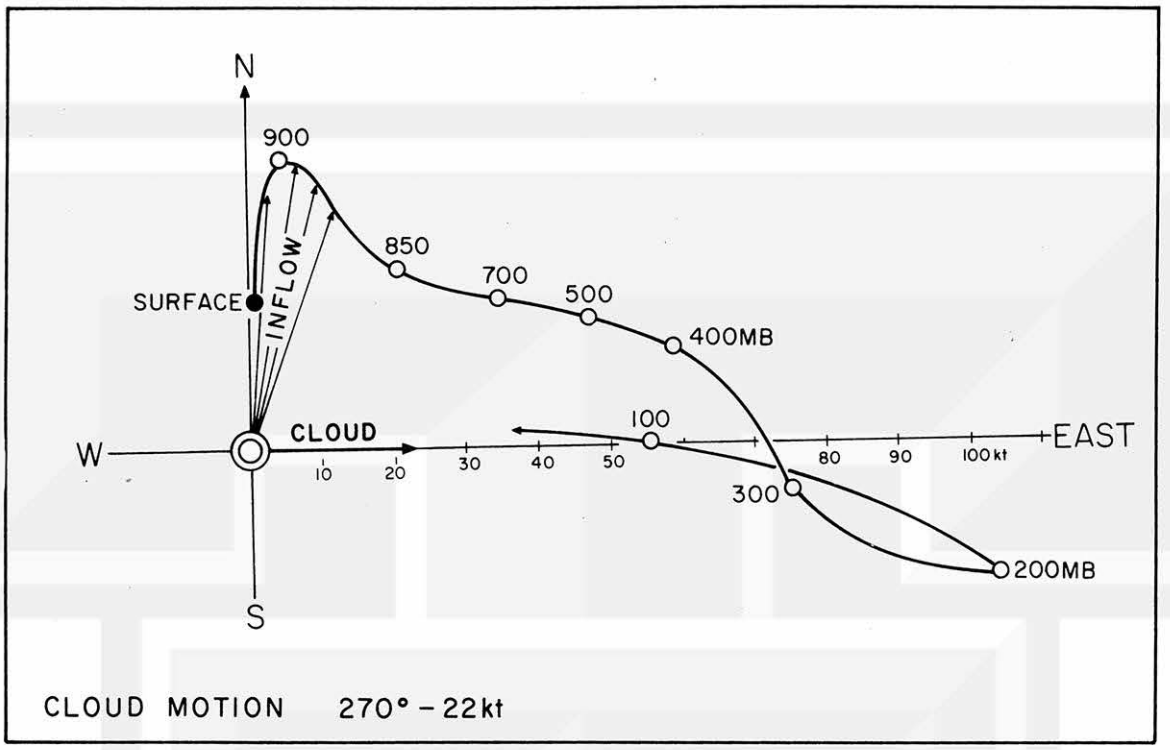

Fig. 5. Hodograph of environmental winds aloft.

4. SURFACE PARAMETERS

The rotating cloud of April 21, 1961 was isolated, while developing very rapidly. The cloud was located near the north end of a warm tongue (see Fig. 6) accompanied by a well-defined moist tongue (see Fig. 7). When such a synoptic situation arises, it is usual to observe a rapid development of thunderstorms in lines. Fortunately, an isolated thunderstorm formed and started rotating shortly afterward. Such a development gave us a golden opportunity for the measurements including multi-directional photographic work. Shown in Fig. 8 are the hourly surface charts including winds, isobars, and stream lines. Note that wind barbs are plotted after doubling the speed; that is, one full barb represents a 5-kt wind. Radar echoes are shown in painted areas. In fact, PPI images from Oklahoma City, Wichita, and Kansas City were used in composite presentations.

A very interesting and important aspect of the storm formation is the existence of a mesoscale field of cyclonic vorticity. At 1600 CST when the cloud just started to precipitate, a significant vorticity and convergence field was in existence. The 1008-mb isobar shows a well defined pressure "pocket". Within one hour, the

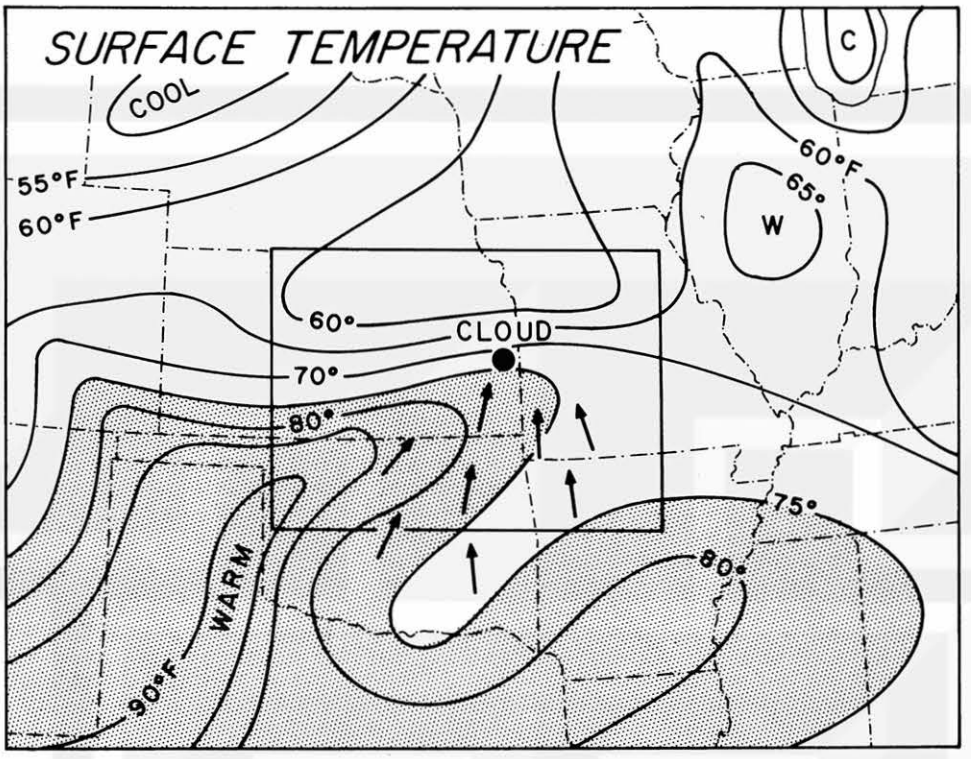

Fig. 6. Distribution of surface temperature. Arrows indicate the inflow directions.

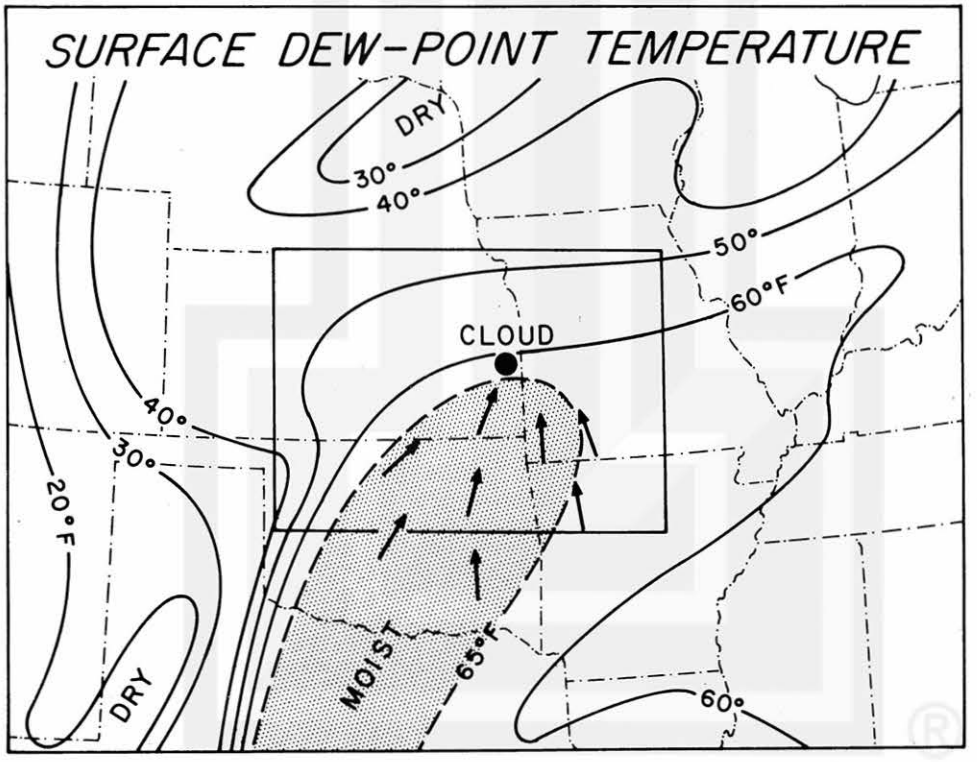

Fig. 7. Distribution of surface dew-point temperature. Hourly surface maps of the boxed area appear in Fig. 8.

pressure pocket deepened considerably, accompanied by a cyclonic flow. The development of a mesocyclone is apparent. The cloud indicated by letter "A" has been growing within the rotating wind field. There were no thunderstorm developments in the vicinity of this cloud.

At 1800, a sudden development of a squall line started to the southwest of the rotating thunderstorm. The development of the line was very fast, thus changing into a full-grown squall line by 1900 CST. As the squall line developed, the isolated cloud "A" weakened very rapidly. The 1900 CST map reveals the major squall-line activities accompanied by a significant convergence extending 300 miles.

This sequence of surface analysis shows that a rotating thunderstorm developed in an area of significant vorticity and convergence. A favorable situation, such as this case, is rather rare because activities usually start in the form of a line, rather than an isolated convection. Moreover, a chance of sending aircraft to such an activity area is often rare, if not remote. The situation used and reported herein occurred in April 1961, about one year after TIROS I. In view of the latest development

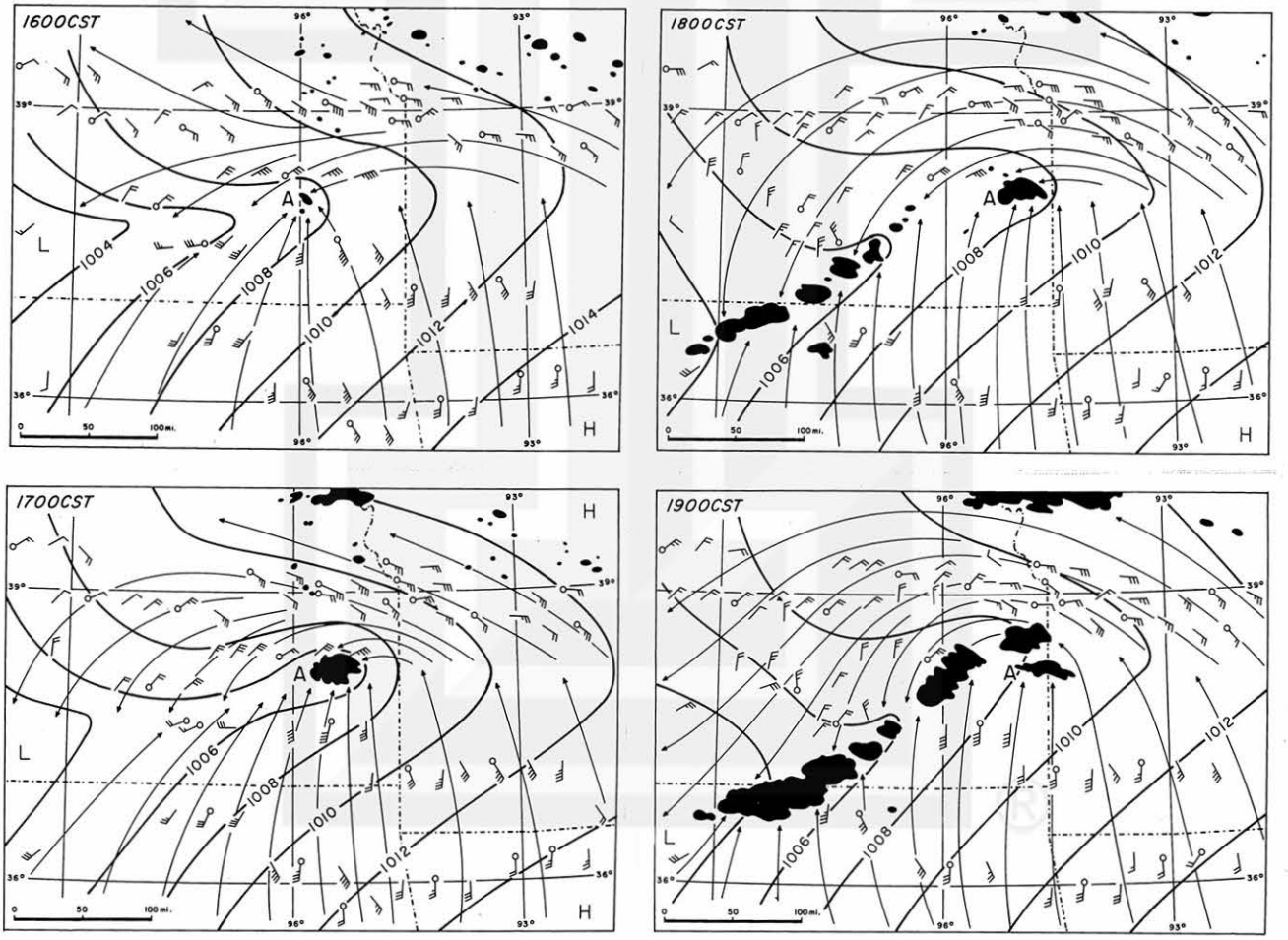

Fig. 8. Hourly surface maps, 1600-1900 CST, April 21, 1961.

of ATS and SMS geostationary satellites, it is expected that research aircraft can be sent to the key spot prior to the development of a rotating cloud.

5. CIRCULATION AROUND THE CLOUD

It is quite unusual to find airborne wind measurement around a rotating cloud. Fortunately, two airplanes were performing research flights beneath and around the cloud under discussion. A B-57, at 45,000 ft, was also in the research mission. However, the wind data were found to be misleading due to an instrument malfunction. For further detail, refer to Fujita and Arnold (1963).

A low-level flight, to obtain Fig. 9, was made by a B-26 with Dr. Chester W. Newton on board. The distribution of 20,000 ft winds presented in Fig. 10 was obtained by the Weather Bureau's DC-6 with Fujita on board. These two charts are the re-analyses of the two-layer flow charts appearing in the original article cited above.

In computing the circulation, both north-south and east-west lines were drawn through the estimated center of the cloud. A system of polar coordinates with 10-km ranges and 10-degree azimuths was used to compute the circulation from

$$\Gamma = \int_0^{360} V \cos\theta \quad r \, d\phi$$

where Γ is the circulation around a circle of radius r, V is the wind velocity at coordinates r, ϕ. To compute the circulation by adding the values for each 10-degree arc, the equation was changed into

$$\Gamma = \frac{\pi r}{18} \sum_{n=1}^{n=36} V_n \cos\theta_n$$

where V_n denotes the wind speed at the n th point and θ_n is the crossing angle.

Such a calculation is very sensitive to the accuracy and smoothing of the field of motion, because the crossing angle reverses the sign of the tangential wind. In order to evaluate the validity of the calculation, the circulation was divided into positive and negative parts,

$$\Gamma = \Gamma^+ + \Gamma^-$$

$$= \frac{\pi r}{18} \left(\sum V_n \cos\theta_n^+ + \sum V_n \cos\theta_n^- \right)$$

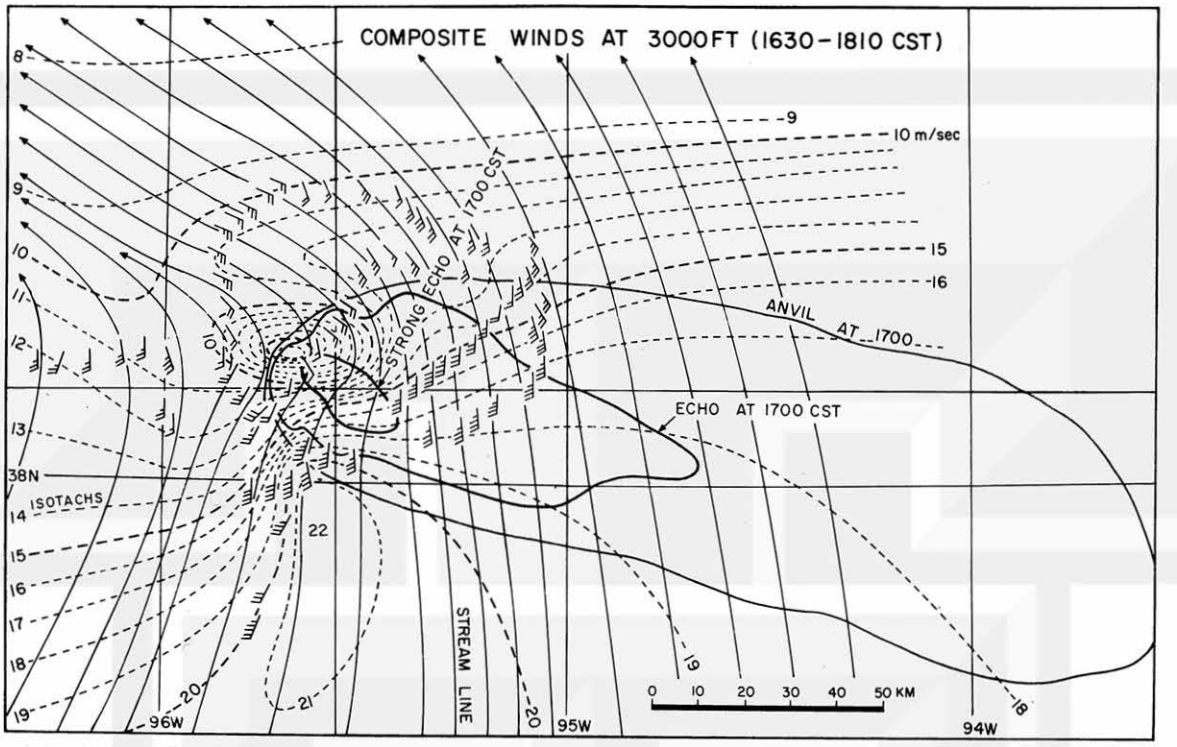

Fig. 9. Streamlines and isotachs at 3,000 ft.

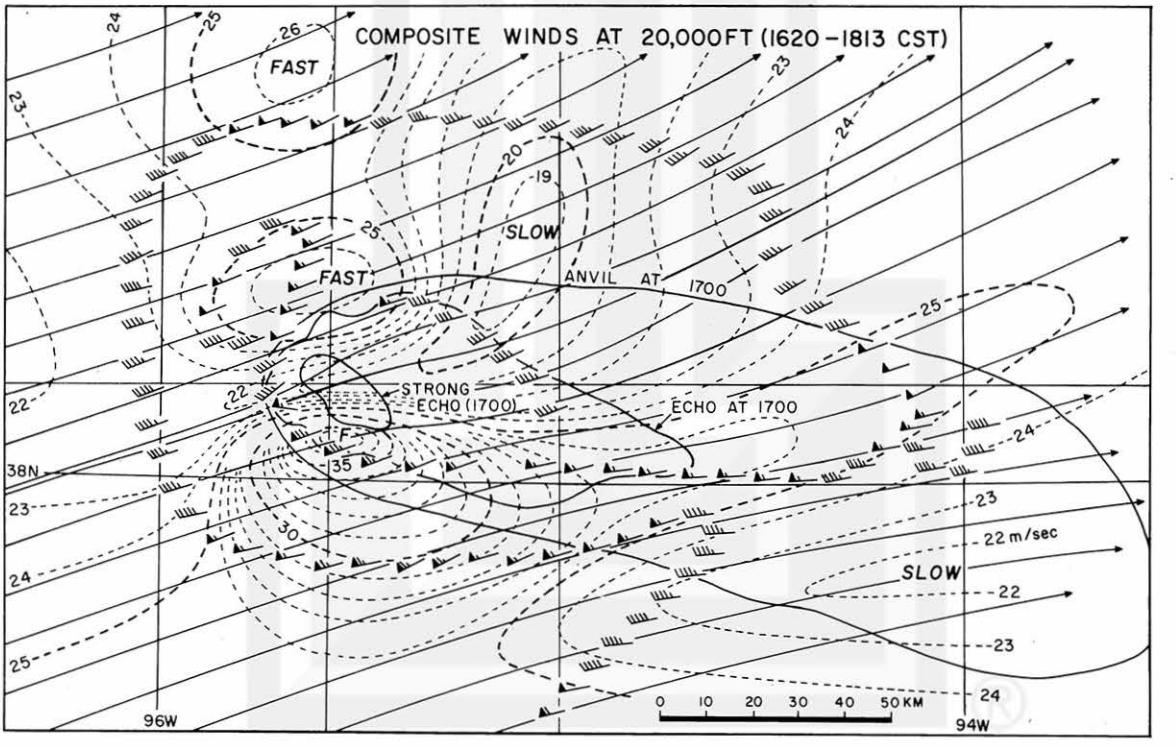

Fig. 10. Streamlines and isotachs at 20,000 ft.

where Γ^+ is the contribution of all the positive tangential velocities while Γ^- is that of all the negative tangential velocities. Since the total circulation is the difference of the absolute values of Γ^+ and Γ^-, the accuracy of the total circulation should be judged by the individual quantities.

For this purpose the positive and negative circulations are tabulated hereunder. Table I reveals that the circulation at 3000 ft is not a small difference of large quantities; hence this calculation of Γ should be accurate. The positive part appears to be more than twice the negative part. The cloud, therefore, must be collecting the cyclonic circulation at the inflow level in order to maintain its rotation.

Table 1. Circulation at 3,000 ft. Unit in 1000 km^2 per hour.

Radius (km)	0	10	20	30	40	50	60	70	80
Positive Γ	0	+1.18	+2.88	+4.61	+6.13	+7.47	+8.72	+9.82	+10.91
Negative	0	-0.52	-1.18	-1.78	-2.15	-2.64	-3.12	-3.60	- 4.02
Total Γ	0	+0.66	+1.70	+2.83	+3.98	+4.83	+5.60	+6.22	+ 6.89
$-\Gamma^+/\Gamma^-$	Unknown	2.27	2.44	2.59	2.85	2.83	2.79	2.72	2.72

The circulation at the higher level may be larger or smaller than that at the 3,000 ft level. If the upper layer is resisting the cloud rotation through viscous coupling, the circulation will decrease upward. If the cloud is fed its rotation from the higher level, while the lower level acts as dissipating media, the circulation will increase upward. Consequently, the evaluation of the circulation at 20,000 ft is of extreme interest.

Table 2. Circulation at 20,000 ft. Unit in 1000 km^2 per hour.

Radius (km)	0	10	20	30	40	50	60	70	80
Positive Γ	0	+2.12	+4.42	+6.25	+7.97	+9.35	+10.97	+12.40	+14.05
Negative Γ	0	-1.74	-3.74	-5.41	-6.82	-8.26	- 9.76	-11.36	-12.80
Total Γ	0	+0.38	+0.68	+0.84	+1.15	+1.09	+ 1.21	+ 1.04	+ 1.25
$-\Gamma^+/\Gamma^-$	Unknown	1.22	1.18	1.15	1.17	1.13	1.12	1.09	1.09

The nature of the circulation at 20,000 ft appears to be quite different from that at 3,000 ft. There, the absolute values of positive and negative circulations are very close to each other, especially when the distance from the cloud is large. This would mean that the cloud is losing its circulation against the irrotational flow. Since the absolute ratio of the circulations is close to 1.00 the accuracy of the computed values could be low for large radii.

The values of the circulation in Tables 1 and 2 are plotted in Fig. 11. It is obvious that the circulation around the cloud at all distances up to 80 km decreases rapidly as the height increases to the 20,000-ft level.

The fact that the circulation increases outward at the 3,000-ft level implies that the inflow field is rotational. Thus the converging air will be maintaining the rotation despite the fact that the frictional dissipation does exist. At the 20,000-ft level, however, there is no rotation within the basic flow in which the cloud is imbedded. The circulation beyond the 40-km radius remains practically the same, meaning that no vorticity exists in the distant environment.

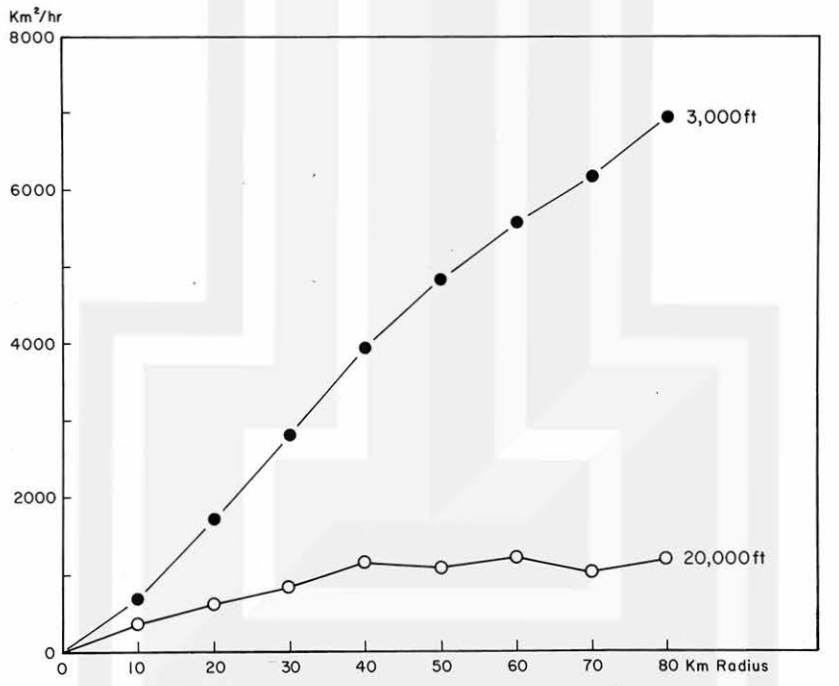

Fig. 11. Circulation around the rotating thunderstorm of April 21, 1961, at the 3,000 and 20,000 ft levels.

6. TEMPERATURE OF CLOUD

Since the strong echo region of the rotating cloud of April 21, 1961 was not penetrated by any research aircraft, it is very difficult to establish the in-cloud temperature through direct measurements.

One of the indirect means is to assume the moist-adiabatic ascent without entrainment. Such an assumption is entirely wrong for small cumulus-type clouds. For a rotating thunderstorm of this size, however, the no-entrainment assumption is not too far from being realistic, because the entrainment is in the order of several per cent.

The moist adiabat of the incloud updraft can be determined from the air temperature and the dew-point temperature of the inflow air. Figures 6 and 7 are, thus, used to obtain

Inflow air temperature	75°F (24°C)
Inflow dew-point temperature ...	65°F (18°C)
Station pressure	950 mb

When the inflow air is lifted adiabatically, condensation will take place at the 900-mb level. The temperature distributions computed from the moist-adiabatic assumption and the environmental temperature from Fig. 4 are given in Table 3.

Table 3. Vertical distribution of in-cloud and environmental temperature. Temperature difference denotes the in-cloud temperature less the environmental temperature.

Height	Pressure	In-cloud Temp.	Env. Temp.	Difference
SFC	980 mb	--	+23.7°C	--
1 km	900	+17.0°C	+19.0	-2.0°C
2	810	+12.7	+13.0	-0.3
3	710	+ 7.8	+ 5.9	+1.9
4	630	+ 2.6	- 0.3	+2.9
5	560	- 2.7	- 6.7	+4.0
6	490	- 8.5	-12.8	+4.3
7	430	-14.8	-20.4	+5.6
8	370	-23.0	-29.0	+6.0
9	320	-31.0	-37.7	+6.7
10	280	-40.0	-47.2	+7.2
11	240	-49.2	-54.0	+4.8
12	205	-58.6	-55.7	-2.9

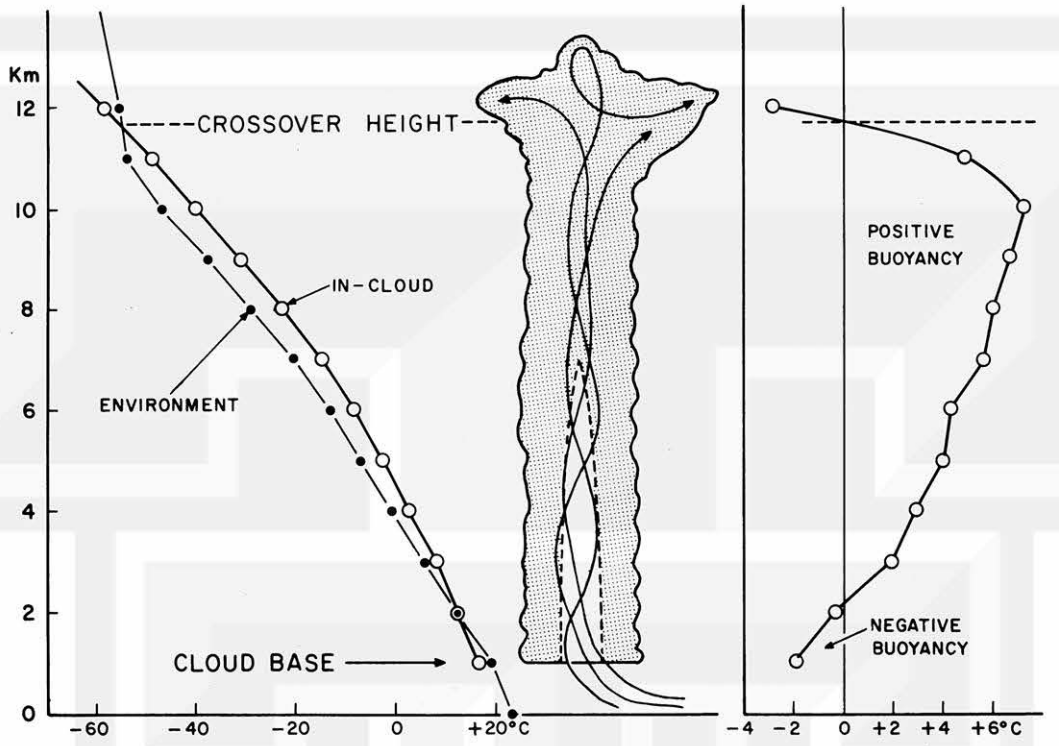

Fig. 12. Vertical distribution of temperature. In-cloud temperatures were computed from the moist adiabat.

A schematic diagram of the rotating cloud and the temperature distribution is shown in Fig. 12. The temperature difference, which is an indicator of the buoyancy, appears to be negative to about the 2-km level. Such negative buoyancy is a common feature of large convective clouds over the Midwest.

The updraft in its first phase will have to receive the dynamical forces necessary to penetrate through the layer of negative buoyancy. One of the forces is provided by frictional convergence within the mesoscale pressure field, which may be called the pressure pocket. Another possible force is the vertical gradient of the non-hydrostatic pressure created by the rising mass of the rotating cloud.

The hen-and-egg problem exists when the non-hydrostatic pressure is examined in detail. In reality, however, the frictional convergence is the initial force giving rise to the formation of a group of small convective clouds within the pressure pocket. When and if these small clouds amalgamate into a large,tall cloud, the upper-level buoyancy will result in a mass deficit inside the lower parts of the cloud. The deficit naturally results in the vertical and horizontal gradient of the non-hydrostatic pressure.

7. CONCLUSIONS

Rotating thunderstorms have been thought to be a rare form of severe convection. Recent studies indicate, however, that thunderstorms as a whole, or a small portion thereof, rotate more often than one would expect.

Dynamical and thermodynamical aspects of thunderstorms in rotation must be studied in detail. An important aspect of this investigation is the tilt of the axis of rotation which has been assumed to be vertical for most practical purposes. The evidence of tilt as reported in this paper is useful in developing a physical model of a rotating thunderstorm imbedded inside a veering and shearing wind environment. Meanwhile, intensive observations and measurements should be encouraged in an attempt to learn more about the nature of these rotating thunderstorms.

Acknowledgement: The author is grateful to Dr. Robert C. Costen of NASA Langley Research Center for his suggestions in completing this research.

References

Brown, R. A., D. W. Burgess, and K. C. Crawford (1973): Twin Tornado Cyclones Within a Severe Thunderstorm: Single Doppler Radar Observations. Weatherwise, 26, 63-70.

Browning, K. A. (1965): Some Inferences About the Updraft within a Severe Local Storm. J. Atmospheric Sci. 22, 669-677.

Costen, R. C. (1972): Theory for the Drift of Severe Local Storms and Hurricanes. EOS Transactions, AGU, Vol. 53, 988.

Fujita, T. T. (1958): Mesoanalysis of the Illinois Tornadoes of 9 April 1953. J. Meteor., 15, 288-296.

Fujita, T. T. (1960): A Detailed Analysis of the Fargo Tornadoes of June 20, 1957. Research Paper 42, U. S. Weather Bureau.

Fujita, T. T. and J. Arnold (1963): Preliminary Result of Analysis of the Cumulonimbus Cloud of April 21, 1961. SMRP Research Paper 16, 16 pp.

Fujita, T. T. (1965): Formation and Steering Mechanisms of Tornado Cyclones and Associated Hook Echoes. Mon. Wea. Rev., 93, 67-78.

Huff, F. A., H. W. Hiser, and S. G. Bigler (1954): Study of an Illinois Tornado Using Radar, Synoptic Weather and Field Survey Data. Rep. of Investigation No. 22, Ill. State Water Survey.

MESOMETEOROLOGY PROJECT - - - RESEARCH PAPERS

(Continued from front cover)

42.* A Study of Factors Contributing to Dissipation of Energy in a Developing Cumulonimbus - Rodger A. Brown and Tetsuya Fujita

43. A Program for Computer Gridding of Satellite Photographs for Mesoscale Research - William D. Bonner

44. Comparison of Grassland Surface Temperatures Measured by TIROS VII and Airborne Radiometers under Clear Sky and Cirriform Cloud Conditions - Ronald M. Reap

45. Death Valley Temperature Analysis Utilizing Nimbus I Infrared Data and Ground-Based Measurements - Ronald M. Reap and Tetsuya Fujita

46. On the "Thunderstorm-High Controversy" - Rodger A. Brown

47. Application of Precise Fujita Method on Nimbus I Photo Gridding - Lt. Cmd. Ruben Nasta

48. A Proposed Method of Estimating Cloud-top Temperature, Cloud Cover, and Emissivity and Whiteness of Clouds from Short- and Long-wave Radiation Data Obtained by TIROS Scanning Radiometers - T. Fujita and H. Grandoso

49. Aerial Survey of the Palm Sunday Tornadoes of April 11, 1965 - Tetsuya Fujita

50. Early Stage of Tornado Development as Revealed by Satellite Photographs - Tetsuya Fujita

51. Features and Motions of Radar Echoes on Palm Sunday, 1965 - D. L. Bradbury and T. Fujita

52. Stability and Differential Advection Associated with Tornado Development - Tetsuya Fujita and Dorothy L. Bradbury

53. Estimated Wind Speeds of the Palm Sunday Tornadoes - Tetsuya Fujita

54. On the Determination of Exchange Coefficients: Part II - Rotating and Nonrotating Convective Currents - Rodger A. Brown

55. Satellite Meteorological Study of Evaporation and Cloud Formation over the Western Pacific under the Influence of the Winter Monsoon - K. Tsuchiya and T. Fujita

56. A Proposed Mechanism of Snowstorm Mesojet over Japan under the Influence of the Winter Monsoon - T. Fujita and K. Tsuchiya

57. Some Effects of Lake Michigan upon Squall Lines and Summertime Convection - Walter A. Lyons

58. Angular Dependence of Reflection from Stratiform Clouds as Measured by TIROS IV Scanning Radiometers - A. Rabbe

59. Use of Wet-beam Doppler Winds in the Determination of the Vertical Velocity of Raindrops inside Hurricane Rainbands - T. Fujita, P. Black and A. Loesch

60. A Model of Typhoons Accompanied by Inner and Outer Rainbands - Tetsuya Fujita, Tatsuo Izawa, Kazuo Watanabe and Ichiro Imai

61. Three-Dimensional Growth Characteristics of an Orographic Thunderstorm System - Rodger A. Brown

62. Split of a Thunderstorm into Anticyclonic and Cyclonic Storms and their Motion as Determined from Numerical Model Experiments - Tetsuya Fujita and Hector Grandoso

63. Preliminary Investigation of Peripheral Subsidence Associated with Hurricane Outflow - Ronald M. Reap

64. The Time Change of Cloud Features in Hurricane Anna, 1961, from the Easterly Wave Stage to Hurricane Dissipation - James E. Arnold

65. Easterly Wave Activity over Africa and in the Atlantic with a Note on the Intertropical Convergence Zone during Early July 1961 - James E. Arnold

66. Mesoscale Motions in Oceanic Stratus as Revealed by Satellite Data - Walter A. Lyons and Tetsuya Fujita

67. Mesoscale Aspects of Orographic Influences on Flow and Precipitation Patterns - Tetsuya Fujita

68. A Mesometeorological Study of a Subtropical Mesocyclone -Hidetoshi Arakawa, Kazuo Watanabe, Kiyoshi Tsuchiya and Tetsuya Fujita

69. Estimation of Tornado Wind Speed from Characteristic Ground Marks - Tetsuya Fujita, Dorothy L. Bradbury and Peter G. Black

70. Computation of Height and Velocity of Clouds from Dual, Whole-Sky, Time-Lapse Picture Sequences - Dorothy L. Bradbury and Tetsuya Fujita

71. A Study of Mesoscale Cloud Motions Computed from ATS-I and Terrestrial Photographs - Tetsuya Fujita, Dorothy L. Bradbury, Clifford Murino and Louis Hull

72. Aerial Measurement of Radiation Temperatures over Mt. Fuji and Tokyo Areas and Their Application to the Determination of Ground- and Water-Surface Temperatures - Tetsuya Fujita, Gisela Baralt and Kiyoshi Tsuchiya

73. Angular Dependence of Reflected Solar Radiation from Sahara Measured by TIROS VII in a Torquing Maneuver - Rene Mendez.

74. The Control of Summertime Cumuli and Thunderstorms by Lake Michigan During Non-Lake Breeze Conditions - Walter A. Lyons and John W. Wilson

75. Heavy Snow in the Chicago Area as Revealed by Satellite Pictures - James Bunting and Donna Lamb

76. A Model of Typhoons with Outflow and Subsidence Layers - Tatsuo Izawa

* out of print

(continued on outside back cover)

SATELLITE AND MESOMETEOROLOGY RESEARCH PROJECT --- PAPERS

77. Yaw Corrections for Accurate Gridding of Nimbus HRIR Data - R. A. Madden

78. Formation and Structure of Equatorial Anticyclones caused by Large-Scale Cross Equatorial Flows determined by ATS I Photographs - T. T. Fujita, K. Watanabe and T. Izawa

79. Determination of Mass Outflow from a Thunderstorm Complex using ATS III Pictures - T. T. Fujita and D. L. Bradbury

80. Development of a Dry Line as shown by ATS Cloud Photography and verified by Radar and Conventional Aerological Data - D. L. Bradbury

81. Dynamical Analysis of Outflow from Tornado-Producing Thunderstorms as revealed by ATS III Pictures - K. Ninomiya

*82. Computation of Cloud Heights from Shadow Positions through Single Image Photogrammetry of Apollo Pictures - T. T. Fujita

83. Aircraft, Spacecraft, Satellite and Radar Observations of Hurricane Gladys, 1968 - R. C. Gentry, T. Fujita and R. C. Sheets

84. Basic Problems on Cloud Identification related to the design of SMS-GOES Spin Scan Radiometers - T. T. Fujita

85. Mesoscale Modification of Synoptic Situations over the Area of Thunderstorms' Development as revealed by ATS III and Aerological Data - K. Ninomiya

86. Palm Sunday Tornadoes of April 11, 1965 - T. T. Fujita, D. L. Bradbury and C. F. Van Thullenar (Reprinted from Mon. Wea. Rev., 98, 29-69, 1970)

87. Patterns of Equivalent Blackbody Temperature and Reflectance of Model Clouds computed by changing Radiometer's Field of View - J. J. Tecson

88. Lubbock Tornadoes of 11 May 1970 - T. T. Fujita

89. Estimate of Areal Probability of Tornadoes from Inflationary Reporting of their Frequencies - T. T. Fujita

90. Application of ATS III Photographs for determination of Dust and Cloud Velocities over Northern Tropical Atlantic - T. T. Fujita

91. A Proposed Characterization of Tornadoes and Hurricanes by Area and Intensity - T. T. Fujita

92. Estimate of Maximum Wind Speeds of Tornadoes in Three Northwestern States - T. T. Fujita

93. In- and Outflow Field of Hurricane Debbie as revealed by Echo and Cloud Velocities from Airborne Radar and ATS-III Pictures - T. T. Fujita and P. G. Black (Reprinted from Preprint of Radar Meteorology Conference, Nov. 17-20, 1970, Tucson, Arizona)

94. Characterization of 1965 Tornadoes by their Area and Intensity - J. J. Tecson

*95. Computation of Height and Velocity of Clouds over Barbados from a Whole-Sky Camera Network - R. D. Lyons

96. The Filling over Land of Hurricane Camille, August 17-18, 1969 - D. L. Bradbury

97. Tornado Occurrences related to Overshooting Cloud-Top Heights as determined from ATS Pictures - T. T. Fujita

98. FPP Tornado Scale and its Applications - T. T. Fujita and A. D. Pearson

99. Preliminary Results of Tornado Watch Experiment 1971 - T. T. Fujita, J. J. Tecson and L. A. Schaal

100. F-Scale Classification of 1971 Tornadoes - T. T. Fujita

101. Typhoon-Associated Tornadoes in Japan and new evidence of Suction Vortices in a Tornado near Tokyo - T. T. Fujita

102. Proposed Mechanism of Suction Spots accompanied by Tornadoes - T. T. Fujita

103. A Climatological Study of Cloud Formation over the Atlantic during Winter Monsoon - H. Shitara

**104. Statistical Analysis of 1971 Tornadoes - E. W. Pearl

105. Estimate of Maximum Windspeeds of Tornadoes in Southernmost Rockies - T. T. Fujita

106. Use of ATS Pictures in Hurricane Modification - T. T. Fujita

107. Mesoscale Analysis of Tropical Latin America - T. T. Fujita

108. Tornadoes Around The World - T. T. Fujita (Reprinted from Weatherwise, 26, No. 2, April 1973)

109. A Study of Satellite-Observed Cloud Patterns of Tropical Cyclones - E. E. Balogun

110. METRACOM System of Cloud-Velocity determination from Geostationary Satellite Pictures - Y. M. Chang, J. J. Tecson and T. T. Fujita

111. Proposed Mechanism of Tornado Formation from Rotating Thunderstorm - T. T. Fujita

112. Joliet Tornado of April 6, 1972 - E. W. Pearl

113. Results of FPP Classification of 1971 and 1972 Tornadoes - T. T. Fujita and A. D. Pearson

114. Satellite-Tracked Cumulus Velocities - T. T. Fujita, E. W. Pearl and W. E. Shenk

115. General and Local Circulation of Mantle and Atmosphere toward Prediction of Earthquakes and Tornadoes - T. T. Fujita and K. Fujita

116. Cloud Motion Field of Hurricane Ginger during the Seeding Period as determined by the METRACOM System - J. J. Tecson, Y. M. Chang and T. T. Fujita

117. Overshooting Thunderheads observed from ATS and Learjet - T. T. Fujita

118. Thermal and Dynamical Features of a Thunderstorm with a Tilted Axis of Rotation - T. T. Fujita

119. Characteristics of Anvil-Top Associated with the Poplar Bluff Tornado of May 7, 1973 - E. W. Pearl

120. Jumbo Tornado Outbreak of 3 April 1974 - T. T. Fujita

121. Cloud Velocities Over The North Atlantic Computed From ATS Picture Sequences - Y. M. Chang and J. J. Tecson

122. Analysis of Anvil Growth For ATS Pictures - Y. M. Chang

123. Evaluation of Tornado Risk Based On F-Scale Distribution - E. W. Pearl

124. Superoutbreak Tornadoes Of April 3, 1974 As Seen In ATS Pictures - T. T. Fujita and G. S. Forbes